Chapter 3

Analysis of Electrochemical and Structurally Enhanced $LiMn_2O_4$ Nanowire Cathode System

Natasha Ross, Shane Willenberg and
Emmanuel Iwuoha

Additional information is available at the end of the chapter

http://dx.doi.org/10.5772/0

Abstract

The performance of the battery cathode depends on the electrode microstructure and morphology, as well as the inherent electrochemical properties of the cathode materials. The spinel $LiMn_2O_4$ is the most promising candidate as a cathode material because of its low cost and nontoxicity compared with commercial $LiCoO_2$. However, there is still a challenge to synthesize high-quality single-crystal nanostructured cathode materials. Nanowires offer advantages of a large surface to volume ratio, efficient electron conducting pathways and facile strain relaxation. To enhance the activity and stability, flexible spinel nanowires are synthesized, via α-MnO_2 nanowire precursor method. Ultrathin $LiMn_2O_4$ nanowires with cubic spinel structure were synthesized by using a solvothermal reaction to produce α-MnO_2 nanowire followed by solid-state lithiation. $LiMn_2O_4$ nanowires have diameters less than 10 nm and lengths of several micrometers. The $LiMn_2O_4$ nanowires are used as stabilizing support during the electrochemical redox processes. The unique nanoporous material effectively accommodates structural transformation during Li^+ ion insertion and effectively reduces Li^+ diffusion distances, reducing the volumetric changes and lattice stresses during charge and discharge. Galvanostatic battery testing showed that $LiMn_2O_4$ nanowires delivered 146 mAh/g in a large potential window. The electrochemical and spectrochemical interrogation techniques demonstrated that $LiMn_2O_4$ nanowires are promising cathode materials for lithium ion batteries as apposed to $LiMn_2O_4$ powders.

Keywords: electrochemistry, cathode, energy, nanowire, diffusion

1. Introduction

The energy storage field faces a critical challenge: namely, the development of rechargeable systems for load leveling applications (e.g. storing solar and wind energy). Among the available battery technologies to date, only Li-ion batteries may possess the power and energy densities necessary for high power applications. The Li ion battery interface materials can store a lot of Li ions but have large structure change and volume expansion, which can cause mechanical failure. In this work we exploited the use of nanowire (NW) cathode morphology to alleviate these issues. Nanowires offer advantages of a large surface to volume ratio, efficient electron conducting pathways and facile strain relaxation [1]. In lithium-ion batteries, the cathode plays a critical role in determining energy density. Here the main requirements are a prolonged cycle life, components (i.e., relevant elements) abundant in high quantities in the earth's crust, and environmentally friendly systems [2, 3]. Among the commonly used layered Ni or Co oxide materials, the spinel $LiMn_2O_4$ appears to be a more favorable cathode in lithium ion batteries [4]. Spinel $LiMn_2O_4$ is economical, nontoxic and a highly abundant material with superior safety [5]. Conversely, its common drawback is a kinetic limitation, which is observed under fast scan rate or high current density, when the characteristic two peaks/plateaus associated with the charge and discharge mechanism of the spinel structure diminishes. To overcome this obstacle and permit the use of $LiMn_2O_4$ in energy-demanding applications, the use of nanostructured morphologies for the development of fast kinetic electrodes is an ideal approach [6]. Literature studies have shown that the one-dimensional nanosized materials have faster kinetics and higher rate capability than micrometer-sized materials due to the large surface-to-volume ratio that enhances the contact between active material grains and electrolyte. However, the high- temperature sintering process, which is necessary for high-performance cathodes based on high-quality crystallinity, such as $LiMn_2O_4$ leads to large grain size and aggregation which alters the battery performance due to increased lithium ion diffusion length and decreased effective surface area contact with electrolyte. Here, the objective was to produce a highly crystalline nanostructured cathode electrode material. Single crystalline nanowire morphology has proven most appealing because the untwined material fabricated by the single crystalline nanowire reduces aggregation, electronic resistance and grain growth at elevated temperature [7]. Generally, the electrochemical performances of electrode materials are strongly influenced by the phase crystallinity, purity, particle size, and distribution. The internal channels in these nano-crystalline cathode material spheres serve two purposes. They admit liquid electrolyte to allow rapid entry of Li^+ ions for quick battery charging, and they provide space to accommodate expansion and contraction during Li^+ intercalation and deintercalation, boosting battery power characteristics critical to improve the $LiMn_2O_4$ performance. This research work produced highly crystalline $LiMn_2O_4$ nanowires, synthesized using a facile, easy to scale up process, starting with the preparation of R-MnO_2 nanowires followed by solid state reaction with LiOH. Concomitantly, $LiMn_2O_4$ powders were also prepared and studied as comparison [8]. The high rate capability as well as phase stability of the nanowires architecture and electrochemistry was demonstrated as probed by electrochemical and spectrochemical characterization techniques. Because determination of

http://dx.doi.org/10.5772/0

the local structure seems one of the key issue for understanding electrochemical properties, vibrational spectroscopy was also applied to provide information on structural features of the nanowires.

2. Experimental procedure

2.1. Modified $LiMn_2O_4$ nanowire syntheses

In this work, the spinel $LiMn_2O_4$ powders were prepared following a procedure found in the literature with minor adjustments [9]. Typical synthesis includes the reaction of lithium hydroxide and manganese acetate (LiOH and Mn $(CH_3COO)_2$) via a co-precipitation method. A stoichiometric amount of LiOH and $Mn(CH_3COO)_2$ with the cationic ratio of Li/Mn = 1:2 were dissolved in deionized water and mixed by stirring. The solution is then evaporated at 100°C for 10 h to obtain the precursor powder [10]. Concomitantly we effectively produced ultrathin spinel $LiMn_2O_4$ nanowires using a facile, two-step process. First, single crystals were produced from a nonaqueous solution in an autoclave reaction to prepare R-MnO_2 nanowires, followed by solid state reaction with LiOH. In a typical process, a hydroalcoholic solution was formed in distilled water and adding first $(NH_4)_2SO_4$ with $(NH_4)_2S_2O_8$ and then 1-octanol. The solvothermal reaction was then performed at 140°C for 12 h in an autoclave to obtain α-MnO_2. This was followed by a solid state reaction between R-MnO_2 nanowires and LiOH at low pressure and oxygen atmosphere to achieve the pure $LiMn_2O_4$ nanowire phase. The chemistry of the nanostructures, the crystallinity and phase purity of $LiMn_2O_4$ powders, R-MnO_2 and $LiMn_2O_4$ nanowires were all characterized by X-ray diffraction (XRD), scanning electron microscopy (FE-SEM), high resolution transmission electron microscopy (HR-TEM), electrochemical impedance spectroscopy and Nuclear magnetic resonance spectroscopy (^{7}Li NMR) technique to observe the local magnetic fields around atomic nuclei.

3. Characterization and analysis

The morphology and particle size distribution of $LiMn_2O_4$ nanowire material was analyzed with a Transmission electron microscopy (TEM), taken with a JSM-6700F (JEOL). Raman spectra of all samples were recorded at wavelength of 514.5 nm using a laser-spectrometer (model Jobin-Yvon U1000) equipped with dual monochromators coupled with special filter and emission of an argon-ion laser (model Spectra-Physics 2020). To avoid sample photo-decomposition or denaturation a power density as low as 10 W cm^{-2} was used. NMR was carried out at room temperature on Varian spectrometer (VNMRS WB 500 solids) with an 11.7 T magnet. Magic angle spinning (MAS) NMR experiments were performed using a 6 mm MAS probe. The ^{7}Li resonance frequency was 194.29 MHz with a sample spinning speed of 16 kHz. Single-pulse and echo-pulse sequences were used to acquire all spectra. The amount of lithium detectable in the materials was quantified using 1 M LiCl (116.571 MHz) as an

external reference for chemical. XRD Measurements were carried out with a D8 ADVANCE diffractometer from BRUKER axs using an X-ray tube with copper K-alpha radiation operated at 40 kV and 40 mA and a position sensitive detector, Vantec_1, which enables fast data acquisition. Measurement range: [12–90° in 2 theta], Step size: 0.027° in 2 theta, Measurement time: 1 s/step.

3.1. Electrochemical tests

The Electrochemistry of the $LiMn_2O_4$ nanowire cathode, were carried out with electrodes mounted on coin-cells operating at 30°C. Electrode mixtures were prepared by mixing the oxide powder (70 wt%) with acetylene black (current collector) (20 wt%) and polyvinylidene fluoride (PVdF) binder (10 wt%) in N-methylpyrrolidone (NMP) solvent to form a mixed slurry. The slurry was coated on an aluminum foil, followed by drying in a vacuum oven at 120°C for 48 h and a cathode electrode was formed.

4. Results and discussions

4.1. Surface morphology

4.1.1. Transmission electron microscopy (TEM)

Figure 1a–d shows the TEM micrographs of the crystalline $LiMn_2O_4$ spinel nanowires in the range of 5–20 nm without agglomeration. The wires appear to be highly crystalline and moderately dispersed, which causes the material to possess a larger surface area. These nanowires have diameters of tens of nanometers and lengths up to several micrometers and basically retains the morphology of the precursor MnO_2 nanowires. At higher magnification, **Figure 1c**, nanowires adhering together are observed, which leads to the notion that these nanowires have a fiber-brush aspect. **Figure 1b** is a typical high-resolution electron microscopy (HREM) image clearly displaying the lattice fringes of the material. The SAED patterns along [100] direction of the single crystals are showed in the inset. Bright diffraction spots including (022), (222) and (004) in the [100] zone are generated from the spinel structure with *Fd3m* space group. The images also show single $LiMn_2O_4$ nanowires with distinctive lattice fringes. The discriminable lattice fringes illustrate that the prepared nanowires are single crystals in the area shown. **Figure 2** shows a typical TEM image at a magnification of 2 and 20 nm of $LiMn_2O_4$. The primary particle size of the as-synthesized powders is around 10 nm with visible agglomerations. The as-synthesized and calcined powders typically have surface areas of 18.0 $m^2\ g^{-1}$ measured by BET method [11].

4.1.2. Atomic force microscopy (AFM)

The surfaces of the cathode were observed by high-resolution atomic force microscopy in dried state. **Figure 3** shows 2 × 2 μm^2 dimensional AFM images of $LiMn_2O_4$ nanowires and the

http://dx.doi.org/10.5772/0

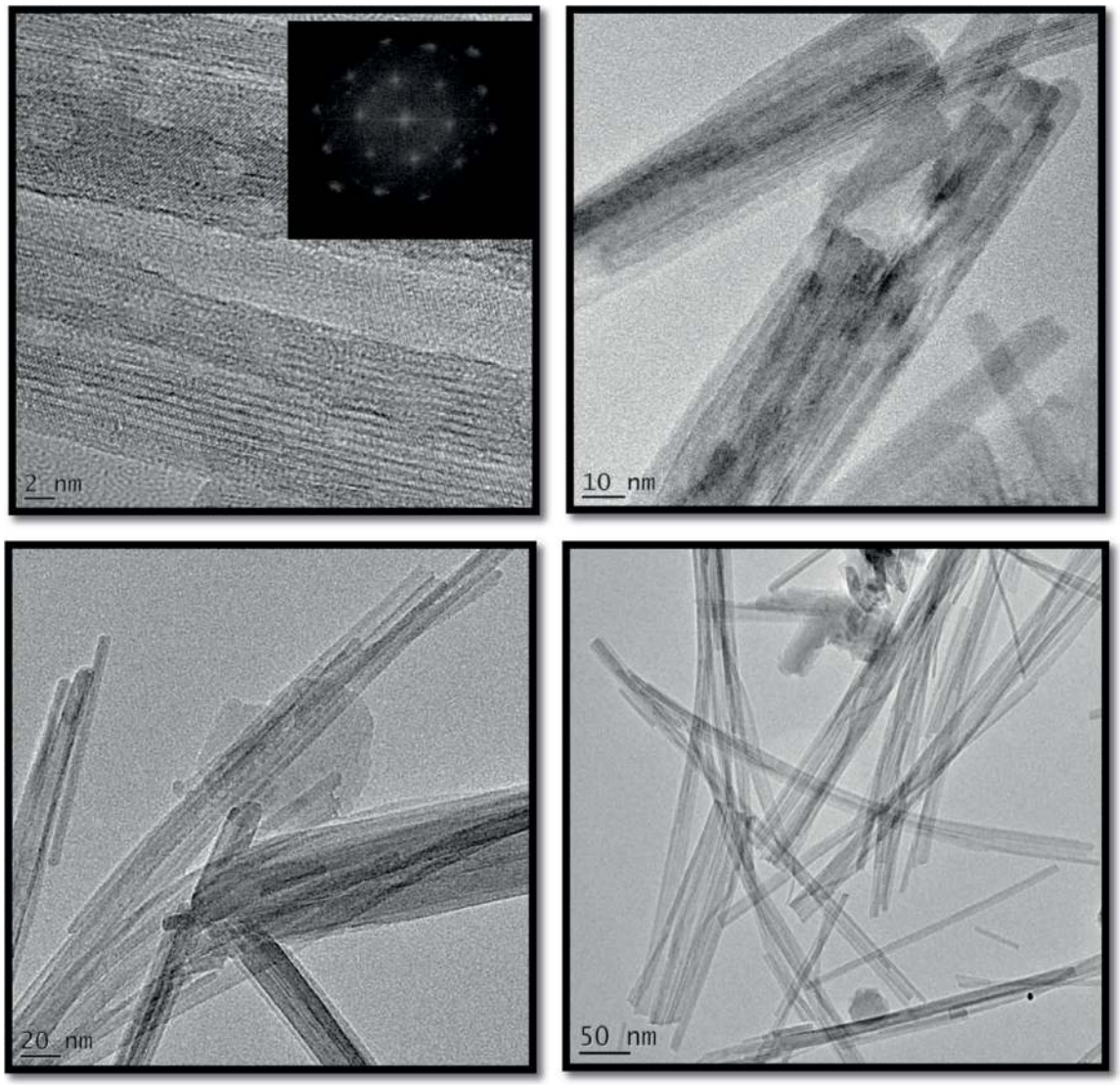

Figure 1. High resolution TEM image of crystalline $LiMn_2O_4$ nanowires.

$LiMn_2O_4$ nanopowders in Ar atmosphere. The images reveal apparent changes in roughness between the films. It is known that the distribution of particles influences the cyclability and discharge capacity [12]. Tapping mode AFM images displayed the surface morphology of nano-$LiMn_2O_4$ particles (a–b). Evidently, a rough structure with closely distributed micropores of less than 5 nm in diameter was observed. From the two-dimensional image, it was evident that this surface yields a large degree of surface roughness (a). A more detailed analysis of the particle size is shown in the histogram of (a, b-i). Particle sizing and metrics play a critical role in determining battery capacity and performance. Therefore, the typical size of materials used for battery construction is >1 μm [13]. Here, the size distribution moved toward an average diameter of 60 nm aiding the high-rate capabilities of the cathode. For $LiMn_2O_4$ several "cauliflower-like" areas are observed with a rms (root mean square) roughness of

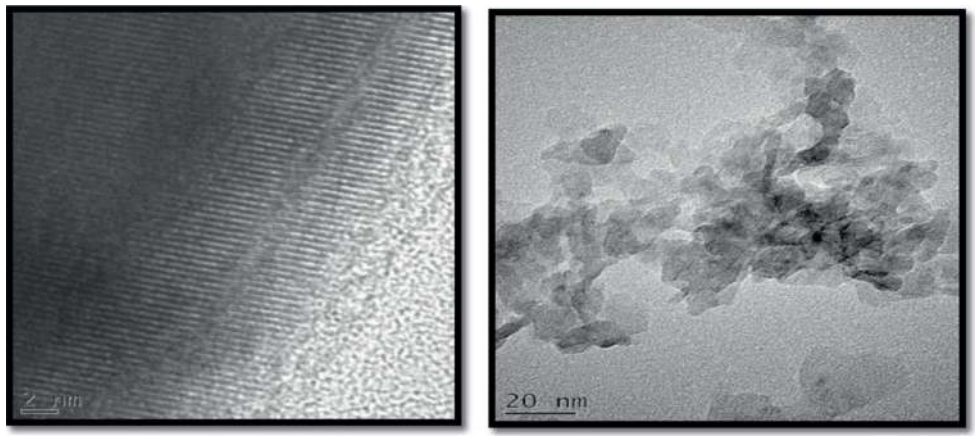

Figure 2. TEM images of $LiMn_2O_4$ nanoparticles.

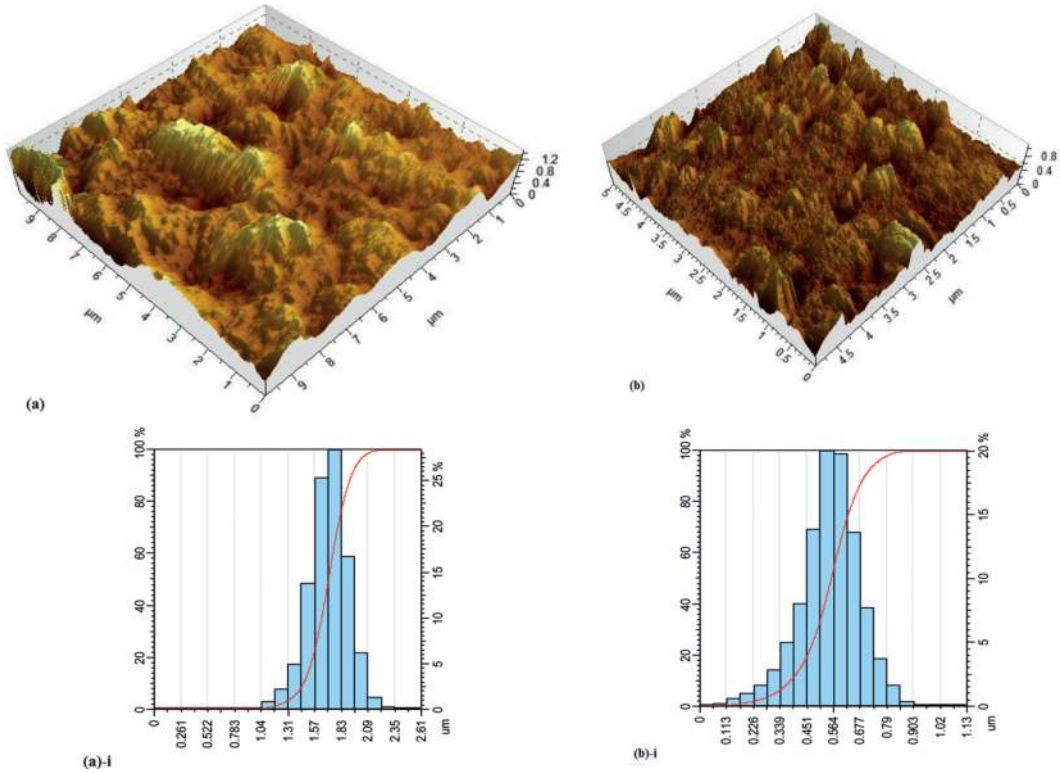

Figure 3. AFM images of $LiMn_2O_4$ shown in tapping mode in three-dimensional views at 600 nm and particle size distribution histogram (i) of $LiMnO_4$ (a) and $LiMn_2O_4$ nanowires (b), respectively.

73.5 Å, whilst $LiMn_2O_4$ nanowires topography appears smoother and homogeneous with rms roughness of 26.3 Å which can be calculated using Eq. (1). These features constitute the stability of the spinel structure, which enhances the electrochemical properties.

$$R_q = \sqrt{\frac{1}{n}\sum_{i=1}^{n} y_i^2} \tag{1}$$

http://dx.doi.org/10.5772/0

4.1.3. Vibrational structure analysis (Raman/SS-NMR)

Figure 4 shows the Raman spectra (RS) of $LiMn_2O_4$ and $LiMn_2O_4$ nanowires. A Blue shift of photons and a noticeable decrease in the peak width is observed with modification. The bands at ~560 and ~660 cm^{-1} are attributed to the O-Mn-O bending and stretching modes, respectively. Some vibrational or rotational transitions, which exhibit low polarizability, becomes Raman inactive therefore sharper peaks signifies better crystallinity and less cation mixing [14]. The observation of narrower bands and less modes may be the result of no translation invariance and lattice distortion around the Mn^{3+} and Mn^{4+} cations. The catalytically active tetragonal hausmannite (Mn_3O_4) spinel is acknowledged by the solid peak erected at 633 cm^{-1}, conforming to the Mn-O breathing vibration of Mn^{2+} ions in tetrahedral coordination (A1g mode) [15]. The T2 g (1), Eg, and T2 g (2) modes of Mn_3O_4 is shown by peaks 300, 347, and 492 cm^{-1} respectively. As discussed by Julien et al. [16], the A1g mode correlated with Mn-O vibration of MnO_6 groups will shift to lower energies as the average Mn oxidation state increases. The Raman data are in agreement with diffraction analysis.

Figure 5 shows the ^{7}Li-NMR spectrums of both spinel $LiMn_2O_4$ and $LiMn_2O_4$ nanowires.

Nuclear magnetic resonance (NMR) spectroscopy has been employed as a significant tool to probe the local structure and dynamics of these nano materials. Here we show how this technique help understand the origins of the performance of the given nanomaterial [17]. $LiMn_2O_4$ is a hopping semiconductor containing both Mn^{3+} and Mn^{4+} ions. The hopping time scale is fast between these ions in comparison to the NMR time scale (ca. 10^{-5} s) and therefore the lithium spins detect a manganese oxidation state corresponding to 3.5 (i.e., "$Mn^{3.5+}$" ions), pertaining to only one magnetically in equivalent lithium site (the 8a site) [12]. This permits the NMR spectroscopy to be used as a means to follow the partial charge-ordering process. The hyperfine shift of >500 ppm from the chemical shift range of diamagnetic compounds containing lithium is characteristic of the ^{7}Li MAS NMR spectrum of $LiMn_2O_4$.

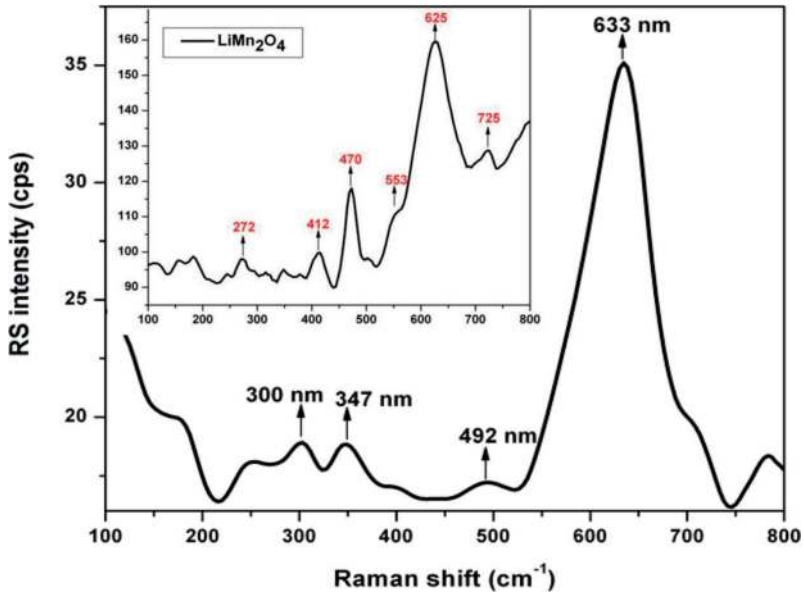

Figure 4. Vibrational spectra of $LiMn_2O_4$ nanowires and $LiMn_2O_4$ precursor (inset).

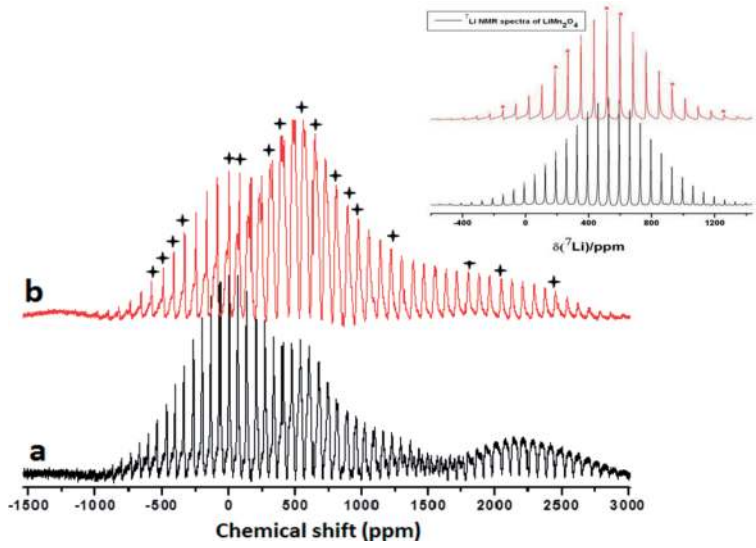

Figure 5. $LiMn_2O_4$ nanowire NMR spectrum at 13 kHz (a) and 16 kHz (b) spinning speed, magnetic field strength of 11.7 T and resonance frequency of 194.29 MHz. $LiMn_2O_4$ nanopowder (inset).

The spinel $LiMn_2O_4$ nanowires have a distinctly different spectral line shape as compared to their powder form [18]. The isotropic resonance at 511 ppm for $LiMnO_4$ is assigned to lithium ions in the tetrahedral 8a site, whilst the isotropic resonances at ~680 and 835 ppm for $LiMn_2O_4$ nanowires is assigned to lithium present in the proximity of higher oxidation state manganese ions (Mn^{4+}). The latter is generally originated from vacancies on both the lithium and manganese sites (i.e., Mn 16*d* sites and the interstitial 16*c* sites or Li-for-Mn substitutions) [19]. The resonance at 445 ppm is ascribed to the presence of Mn^{3+} ions in the Li local coordination sphere. Mn^{3+} is a *Jahn–Teller (distortion)* active ion; therefore there will be a distortion of the octahedron in this case [20]. The enhancement of spinning sideband manifold for $LiMn_2O_4$ nanowires is caused by the increased portion of paramagnetic manganese around lithium [21]. Hence, it can be suggested that the lithium atoms are interacted with the manganese and cause for better electrochemical performance.

4.1.4. X-ray diffraction microscopic analysis (XRD)

The lattice constant was calculated from the corresponding diffraction pattern using XRD spectra, in relation to the crystal structure and is reported in **Figure 6**. All diffraction peaks can be assigned to the diffraction indices of $LiMn_2O_4$ spinel (JCPDS file no. 35-782), indicating that the structure of the spinel was maintained. The majority diffraction peaks of $LiMnO_2$ are observed, and closely correspond to layered $LiMnO_2$ (011), (202) and (111) planes. The intensive diffraction peaks appeared at 21.92, 36.92, 42.42 and 55.96°, respectively, should be assigned to the characteristic peaks for γ-MnO_2, and the peaks occurred at 17.94, 28.78, 66.0°, respectively, should be ascribed to the characteristic peaks for α-MnO_2. Hence, the sample appears to be composed of both γ and α-MnO_2. From the broadening of XRD peaks, it can be said that nanowires are being formed. This suggest that the nanowires would render

http://dx.doi.org/10.5772/0

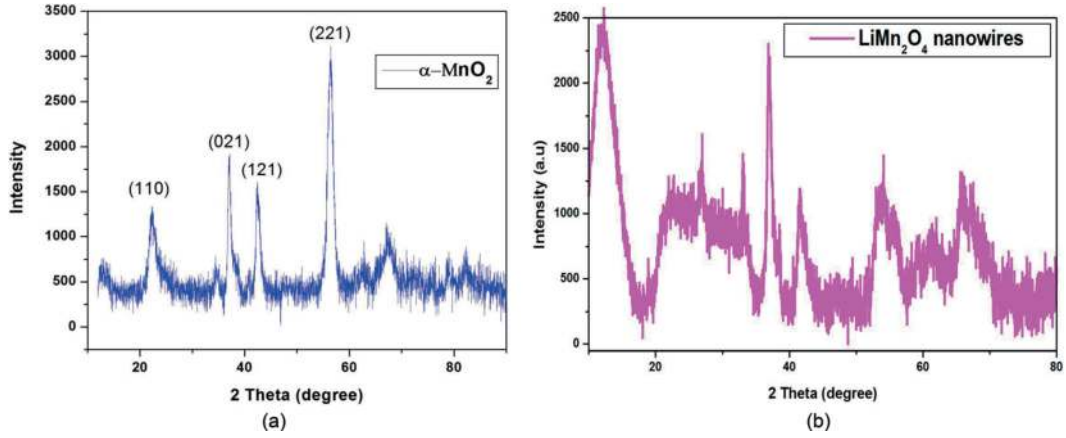

Figure 6. XRD spectra of $LiMn_2O_4$ nanowires (a) and alfa-MnO_2 (b).

unchallenging Li^+ pass through the coating layer more during charging and discharging process as the diffusion path is unhindered [22, 23]. The strong peak at $2\theta = 18.76°$, corresponds to a (111) peak with an interplanar distance of $d = 0.476$ nm. The full width at half-maximum (FWHM) becoming narrower is also due to higher synthesis temperatures which help to enhance the mobility of atoms. Sharp and relatively high intensity peaks (as compared to $LiMn_2O_4$) depicts high crystallinity [24].

4.2. Electrochemical analysis

4.2.1. Redox reaction analysis

To clarify the kinetic behavior of lithium-ion transfer, the discharge tests were carried out at. **Figure 7** shows the effect of discharge current densities on the capacities of the two types of electrodes. It is well known that the nanowire electrodes have good electronic conductivity; therefore, they can greatly increase the electrical conductivity among the transition metal oxide particles and reduce the polarization of the $LiMn_2O_4$ electrode. The nanowire cathode shows an increased discharge current densities due to improvement of Li^+ diffusion pathway [25–27]. This coincides with prior research that has recognized the ability of nanowire architecture to enhance the stability or cyclability of electrode materials [28]. The initial discharge curve of $LiMn_2O_4$ nanowire electrode was similar to that of $LiMn_2O_4$ spinel, due to the lower ratio of Mn^{3+}/Mn^{4+} ions [29]. The initial discharge capacities and corresponding coulombic efficiencies after cycling for the nanowires and $LiMn_2O_4$ were 146 mAh g^{-1} / 99% and 122 mAh g^{-1}/ 70%, respectively. The decrease in capacity over subsequent cycles is explained by the change in surface area [30]. Three-dimensional porous nanostructures with large surface area could exhibit higher durability in the lithium insertion/ extraction process at a high current density, owing to the short lithium ion diffusion lengths in the 3-D channels of the electrode [31]. The $LiMn_2O_4$ nanowire electrode exhibited excellent rate capability as shown in **Figure 7**. The large capacities are due to the nanowire morphology, stability and the high quality of the single crystal, which can shorten the diffusion lengths of both the lithium and electrons [32].

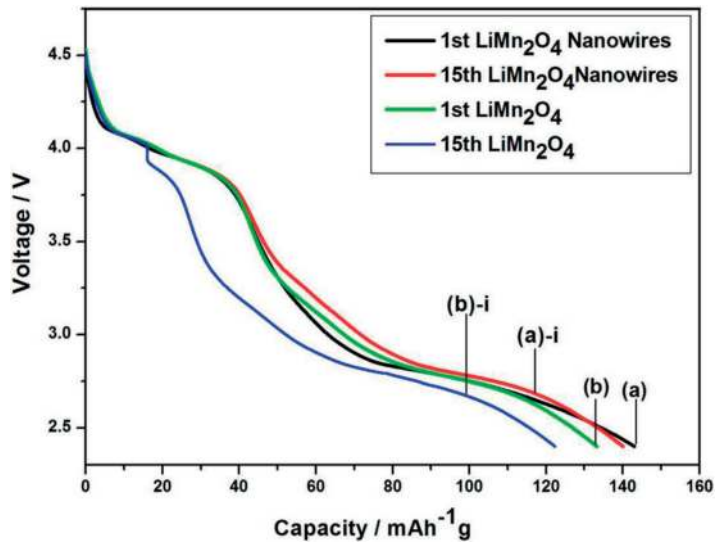

Figure 7. Discharge current densities at 0.1 mV s^{-1} for $LiMn_2O_4$ nanowires (a) and $LiMn_2O_4$ (b) in EC: DMC, 1 M $LiPF_6$ for the (1st (a, b) and 50th (a-i, b-i) cycle).

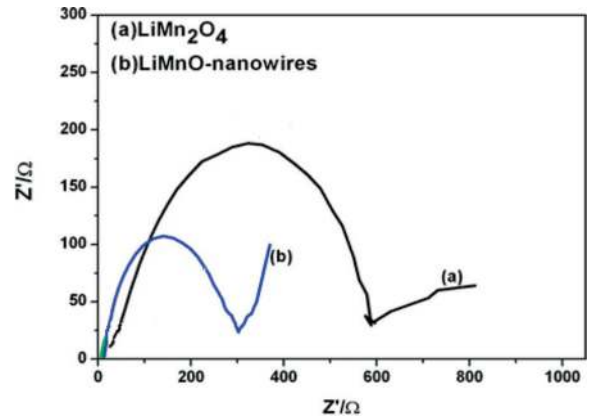

Figure 8. Nyquist plot of $LiMn_2O_4$ (a) and $LiMn_2O_4$ nanowires (b).

This was further corroborated by electrochemical impedance spectroscopy results shown in **Figure 8**. The nanowires show a significant decrease in impedance due to their enhanced electrochemical diffusion processes.

5. Conclusion

In summary, the $LiMn_2O_4$ nanowires have proven excellent thermal stability for a high-temperature sintering process as well as a charge-discharge reversible stability and improved conductivity attained by their architecture, excellent crystallinity and decreased impedance.

http://dx.doi.org/10.5772/0

All the as-prepared powders were identified as a single phase of cubic spinel structure indicative of an unobstructed Li ion diffusion pathway. The results have shown that thin-nanowire precursor morphology is preserved after the solid-state reaction. Such morphology improves the kinetic properties at very high current rate and was capable of the facile structural transformation of the cubic and tetragonal phase in the large compositional range. The $LiMn_2O_4$ nanowires showed a decrease in potential difference, indicating an improved charge transportation process. The nanostructures aid structural stability, reduction of side reactions and Mn dissolution between the interface of the cathode and electrolyte, which contributes to the recovering performance. Moreover, the nanowire cathode system has great potential for improving the electrode-filled ratio and safety in lithium ion battery–operating electronic devices, in transportation applications, and in applications on the electric grid.

Acknowledgements

Natasha Ross is grateful to the National Research Foundation (NRF) for the award of the Department of Science and Technology's Innovation Postgraduate Scholarship for the research grant.

Conflict of interest

The author declares that there is no conflict of interest.

Author details

Natasha Ross*, Shane Willenberg and Emmanuel Iwuoha

*Address all correspondence to: nross@uwc.ac.za

University of the Western Cape, Cape Town, South Africa

References

[1] Marom R, Amalraj SF, Leifer N, Jacob D, Aurbach D. A review of advanced and practical lithium battery materials. Journal of Materials Chemistry. 2011;**21**:9938

[2] Kim YS, Kanoh H, Horotsu T, Ooi K. Chemical bonding of ion-exchange type sites in spinel-type manganese oxides $Li_{1.33}Mn_{1.67}O_4$. Materials Research Bulletin. 2002;**37**:391-396

[3] Thackeray MM, David WIF, Goodenough JB. Lithium insertion into manganese spinels. Materials Research Bulletin. 1983;**18**:641-647

[4] Zhong Q, Bonaldarpour A, Zhang M, Gao Y, Dahn JR. Synthesis and electrochemistry of $LiNi_xMn_{2-x}O_4$. Journal of the Electrochemical Society. 1997;**144**:205

[5] Dokyun K, Hyun-Wook L, Muralidharan P, Cui Y. Spinel $LiMn_2O_4$ nanorods as lithium ion battery cathodes. Nano Letters. 2008;**8**(11):3948-3952

[6] Sun YK, Jeon YS, Leeb HJ. Overcoming Jahn-Teller distortion for spinel Mn phase. Electrochemical and Solid-State Letters. 2000;**3**:7

[7] Hosono E, Kudo T, Honma I, Matsuda H, Zhou H. Synthesis of single crystalline spinel $LiMn_2O_4$ nanowires for a lithium ion battery with high power density. Nano Letters. 2009;**9**(3):1045-1051

[8] Hyun-Wook L, Muralidharan P, Riccardo R, Claudio MM, Yi C, Kyung KD. Ultrathin spinel LiMnO nanowires as high power cathode materials for Li-ion batteries. Nano Letters. 2010;**10**(10):3852-3856

[9] Hui X, Zhentao L, Jianping X. Nanostructured $LiMn_2O_4$ and their composites as high-performance cathodes for lithium-ion batteries. Progress in Natural Science: Materials International. 2012;**22**(6):572-584

[10] Kweon HJ, Kim SJ, Park DG. Modification of $Li_xNi_{1-y}Co_yO_2$ by applying a surface coating of MgO. Journal of Power Sources. 2000;**88**:255-261

[11] Xiuqiang X, Dawei S, Bing S, Jinqiang Z, Chengyin W, Guoxiu W. Synthesis of single-crystalline spinel $LiMn_2O_4$ nanorods for lithium-ion batteries with high rate capability and long cycle life. Chemistry A european Journal. 2014;**20**(51):17125-17131

[12] Wang P, Li YN, Yang J, Zheng Y. Carbon-coated Si-Cu/graphite composite as anode material for lithium-ion batteries. International Journal of Electrochemical Science. 2006; **1**:122-129

[13] Li W, Andrei D, Pilgun O, Hugo C, Suhyeon P, Jaephil C, Arumugam M. Dynamic behaviour of interphases and its implication on high-energy-density cathode materials in lithium-ion batteries. Nature Communications. 2017;**8**:14589

[14] Ramana C, Massot VM, Julien CM. XPS and Raman spectroscopic characterization of $LiMn_2O_4$ spinels. Surface and Interface Analysis. 2005;**34**:412-416

[15] Li TT, Guo CL, Sun B, Li T, Li YG, Hou LF, Wei YH. Ell shaped Mn_3O_4 tetragonal bipyramids with good performance for lithium ion batteries. Journal of Materials Chemistry A. 2015;**3**:7248-7254

[16] Julien CM, Massot M, Poinsignon C. Lattice vibrations of manganese oxides: Part I. Periodic structures. Spectrochimica Acta A. 2004;**60**:689-700

[17] Jordi C, Clare PG. Lithium-ion batteries: Li-6 MAS NMR studies on materials. 2011. DOI: 10.1002/9781119951438.eibc0457

[18] Clare PG, Nicolas D. NMR studies of cathode materials for lithium-ion rechargeable batteries. Chemical Reviews. 2004;**104**:4493-4512

[19] Chi-Hung L, Chun-Wei H, Jui-Yuan C, Chung-Hua C, Tzung CT, Kuo-Chang L, Ming-Yen L, Wen-Wei W. Optoelectronic properties of single-crystalline Zn_2GeO_4 nanowires. Journal of Physical Chemistry C. 2014;**118**(15):8194-8199

[20] Naghash AR, Lee JY. Preparation of spinel lithium manganese oxide by aqueous co-precipitation. Journal of Power Sources. 2000;**85**:284

[21] Lee YJ, Wang F, Crey CP. ^{6}Li and ^{7}Li MAS NMR studies of lithium manganate cathode materials. Journal of the American Chemical Society. 1998;**120**:2601

[22] Byung-Sik M, Jae-Hyeong L, Jung H. Comparative studies of the properties of CdS films deposited on different substrates by R.F. sputtering. Thin Solid Films. 2006;**511**:299-303

[23] Hunter JC. Preparation of a new crystal form of manganese dioxide. Journal of Solid State Chemistry. 1981;**39**:142-147

[24] Eftekhari A. Effects of metal source in metal substitution of lithium manganese oxide spinel. Solid State Communications. 2006;**140**:39

[25] Ni JF, Zhou HH, Chen JT, Zhang XX. $LiFePO_4$ doped with ions prepared by co-precipitation method. Materials Letters. 2005;**59**:2356-2361

[26] Yu L, Cai D, Wang H, Titirici M-M. Synthesis of microspherical $LiFePO_4$-carbon composites for lithium-ion batteries. Nanomaterials. 2013;**3**:443-452

[27] Atanasov M, Barras J-L, Benco L, Daul C. Electronic structure, chemical bonding, and vibronic coupling in Mn^{IV}/Mn^{III} mixed valent $Li_xMn_2O_4$ spinels and their effect on the dynamics of intercalated Li: A cluster study using DFT. Journal of the American Chemical Society. 2000;**122**:4718-4728

[28] Yi T-F, Li C-Y, Zhu Y-R, Zhu R-S, Shu J. Electrochemical intercalation kinetics of lithium ions for spinel $LiNi_{0.5}Mn_{1.5}O_4$ cathode material. Russian Journal of Electrochemistry. 2010;**46**:227-232

[29] Yamada A, Chung S, Hinokuma CK. Optimized $LiFePO_4$ for lithium battery cathodes. Journal of the Electrochemical Society. 2001;**148**:A224

[30] Yin Z, Ma D, Bao XH. Emulsion-assisted synthesis of monodisperse binary metal nanoparticles. Chemical Communications. 2010;**46**:1344-1346

[31] Kim JM, Lee G, Kim BH, Huh YS, Lee G-W, Kim HJ. Ultrasound assisted synthesis of Li-rich mesoporous $LiMn_2O_4$ nano-spheres for enhancing the electrochemical performance in Li-ion secondary batteries. Ultrasonics Sonochemistry. 2012;**19**:627-631

[32] Qu Q, Fu L, Zhan X, Samuelis D, Maier J, Li L, Tian S, Li Z, Wu Y. Porous $LiMn_2O_4$ as cathode material with high power and excellent cycling for aqueous rechargeable lithium batteries. Energy & Environmental Science. 2011;**4**:3985-3990